Negative lateral conductivity of hot electrons in a biased superlattice

A. Hernández-Cabrera* and P. Aceituno
Departamento de Física Básica, Universidad de La Laguna, La Laguna, 38206 Tenerife, Spain and Instituto Universitario de Estudios Avanzados (IUdEA) en Física Atómica, Molecular y Fotónica, Universidad de La Laguna, La Laguna, 38206 Tenerife, Spain

F. T. Vasko†
Institute of Semiconductor Physics, NAS Ukraine, Pr. Nauki 41, Kiev 03028, Ukraine

(Received 18 January 2009; revised manuscript received 18 May 2009; published 8 June 2009)

Nonequilibrium electron distribution in a superlattice subjected to a homogeneous electric field (biased superlattice with equipopulated levels) is studied within the tight-binding approximation, taking into account the scattering by optical and acoustic phonons and by lateral disorder. It is found that the distribution versus the in-plane kinetic energy depends essentially on the ratio between the Bloch energy, ε_B, and the optical phonon energy, $\hbar\omega_0$. The in-plane conductivity is calculated for low-doped structures at temperatures of 4.2 and 20 K. The negative conductivity is found for bias voltages corresponding to $\varepsilon_B/\hbar\omega_0 \simeq 1/2, 1/3, 2/3, \ldots$ (the Bloch-phonon resonance condition).

DOI: 10.1103/PhysRevB.79.235312 PACS number(s): 72.20.Dp, 72.20.Ht, 73.21.Cd

I. INTRODUCTION

Vertical charge transfer in a superlattice (SL) subjected to a homogeneous electric field [biased superlattice (BSL), with equipopulated levels] has been under investigation starting 1970s (see Ref. 1 and references in the reviews in Ref. 2). The stimulated emission in the midinfrared (mid-IR) and terahertz spectral regions, caused by the intersubband transitions of electrons under vertical transport through tunnel-coupled cascade structures (monopolar laser effect), has also been investigated. Using this scheme, both mid-IR and terahertz laser viabilities have been demonstrated during the previous decade (see references in Refs. 3 and 4). Recently, nonequilibrium electron distribution has been observed experimentally[5] and described theoretically[6,7] for heavily doped cascade structures when the effective temperature is determined from the balance equation. To the best of our knowledge, there is no consideration of nonequilibrium carriers for low-doped structures which were performed beyond the balance approach.

In this paper we study the nonequilibrium electron distribution in a BSL under vertical current through the Wannier-Stark ladder, which takes place under the condition $2T \ll \varepsilon_B$, where ε_B is the Bloch energy and T stands for the tunneling matrix element between adjacent quantum wells (QWs).[8] Since the parameters of each QW and the conditions for interwell transitions are identical [see Fig. 1(a)] the level populations over QWs are the same. But the distribution of electrons over the in-plane energy should change essentially due to the interplay between elastic and nonelastic processes [see Figs. 1(b)–1(d)]. In the low-temperature case we only consider the passive region, with energy less than the optical phonon energy, $\hbar\omega_0$. For the low-concentration limit, we consider the kinetic equation which takes into account the quasielastic scattering caused by acoustic phonons as well as the interwell tunneling due to elastic scattering by disorder and due to optical phonon emission. As a result, we obtain the electron distribution versus the in-plane kinetic energy which strongly depends on the ratio $\varepsilon_B/\hbar\omega_0$. In the case of the Bloch-phonon resonance, when $M\varepsilon_B = N\hbar\omega_0$ with N and M as integers, *a partially inverted distribution*, with maxima at energies $(N/M)\hbar\omega_0$, can be realized.

The phenomenon of absolute negative conductivity (ANC) of electrons excited near the energy $\hbar\omega_0$ was discussed four decades ago[9] and different regimes of ANC (including magnetotransport[10] and transient regimes of the response[11]) were considered. Recently, ANC regime was observed when microwave radiation acts on two-dimensional (2D) electrons in a quantizing magnetic field.[12] As shown below, *a resonant ANC regime* of the in-plane response can be obtained in BSL under the Bloch-phonon resonance conditions. Such a peculiarity appears due to the contribution of the energy interval near $\hbar\omega_0$ where an inverted distribution takes place. As a result, BSL becomes instable with respect

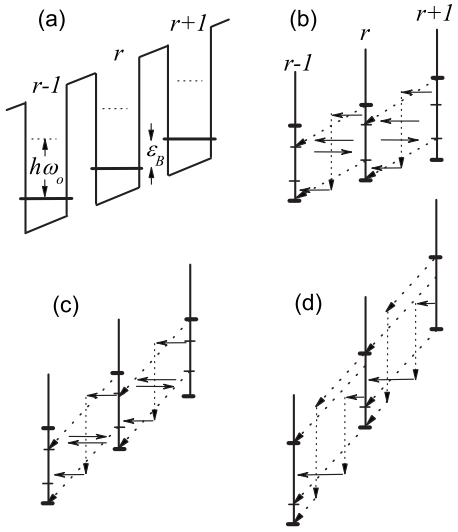

FIG. 1. (a) Band diagram for BSL of period Z with the Bloch energy ε_B which is comparable to the optical phonon energy, $\hbar\omega_0$. [(b)–(d)] Schemes of tunneling transitions due to elastic scattering (solid arrows), spontaneous optical phonon emission (dotted arrow), and phonon emission from the active region (vertical dashed arrows) for the cases (b) $\varepsilon_B < \hbar\omega_0/2$, (c) $\hbar\omega_0/2 < \varepsilon_B < \hbar\omega_0$, and (d) $\hbar\omega_0 < \varepsilon_B$.

to in-plane fluctuations if ANC conditions are satisfied.

The paper is organized as follows. The basic equations describing distribution of hot electrons in BSL and in-plane conductivity are presented in Sec. II. Analytical consideration for the case $\varepsilon_B/\hbar\omega_0=1/2$ (the second-order Bloch-phonon resonance) is performed in Sec. III. Results of numerical calculations are discussed in Sec. IV. Our concluding remarks and the list of assumptions made are given in Sec. V. In Appendix, the kinetic equations for different $\varepsilon_B/\hbar\omega_0$ are presented.

II. BASIC EQUATIONS

Within the tight-binding approximation, the electrons in BSL are characterized by the 2D momentum, $\mathbf{p}$, and the quantum well number, $r=0,\pm 1,\ldots$. Under the in-plane electric field $\mathbf{E}$, the distribution function, $f_{r\mathbf{p}}$, is governed by the system of kinetic equations,

$$e\mathbf{E}\cdot\frac{\partial f_{r\mathbf{p}}}{\partial \mathbf{p}}=\sum_k J_k(f|r\mathbf{p}), \tag{1}$$

where the collision integrals $J_k(f|r\mathbf{p})$ describe the scattering processes caused by the longitudinal optical (LO) phonon emission (k=LO), the acoustic phonons (k=ac), or the static disorder ($k=d$). Below we present these collision integrals and consider the kinetic equation for the distribution functions $f_{r\mathbf{p}}$, which are normalized by the condition $n=(2/V)\Sigma_{r\mathbf{p}}f_{r\mathbf{p}}$, where n is the three-dimensional (3D) concentration, V is the normalization volume, and the factor 2 is due to spin. We also evaluate the lateral current density $\mathbf{I}=(2e/Vm)\Sigma_{r\mathbf{p}}\mathbf{p}f_{r\mathbf{p}}$ for electrons, with the effective mass m, under a weak probe field $\mathbf{E}$.

A. Collision integrals

Here we evaluate the collision integrals in Eq. (1) by modifying the general expressions[13] for electrons in BSL, described in the tight-binding approximation by the states $|r\mathbf{p}\rangle$, with the energies $\varepsilon_{rp}=r\varepsilon_B+\varepsilon_p$, where $\varepsilon_p=p^2/2m$ is the in-plane kinetic energy (see Sec. 3 in Ref. 8). For the low-temperature case, when temperature of phonons $T_{\rm ph}\ll\hbar\omega_0$, the spontaneous emission of dispersionless optical phonons is described by

$$J_{\rm LO}(f|r\mathbf{p})=\frac{2\pi}{\hbar}\sum_{r'\mathbf{p}'\mathbf{Q}}|C_Q^{(\rm LO)}|^2|\langle r'\mathbf{p}'|\,e^{i\mathbf{Q}r}\,|r\mathbf{p}\rangle|^2\times[\delta(\varepsilon_{r'p'}-\varepsilon_{rp}-\hbar\omega_0)f_{r'\mathbf{p}'}-\delta(\varepsilon_{rp}-\varepsilon_{r'p'}-\hbar\omega_0)f_{r\mathbf{p}}], \tag{2}$$

where $|C_Q^{(\rm LO)}|^2$ is the bulk matrix element for the Frölich interaction, with the vibration mode characterized by the 3D wave vector $\mathbf{Q}$, and $|\langle r'\mathbf{p}'|\,e^{i\mathbf{Q}r}\,|r\mathbf{p}\rangle|^2$ is the overlap factor. Taking into account the quasielastic energy relaxation caused by the equipopulated acoustic phonons, one obtains the collision integral

$$J_{\rm ac}(f|r\mathbf{p})=\sum_{r'\mathbf{p}'}W_{r\mathbf{p}r'\mathbf{p}'}(f_{r'\mathbf{p}'}-f_{r\mathbf{p}})-\frac{1}{2}\sum_{r'\mathbf{p}'}\Delta W_{r\mathbf{p}r'\mathbf{p}'}(f_{r'\mathbf{p}'}+f_{r\mathbf{p}}). \tag{3}$$

The transition probabilities $W_{r\mathbf{p}r'\mathbf{p}'}$ and $\Delta W_{r\mathbf{p}r'\mathbf{p}'}$ are written here within the second-order accuracy with respect to the acoustic phonon energy, $\hbar\omega_Q$, as follows:

$$W_{r\mathbf{p}r'\mathbf{p}'}=K_{rr'}(\mathbf{p}-\mathbf{p}')\delta(\varepsilon_{r'p'}-\varepsilon_{rp})+\frac{T_{\rm ph}}{2}\Delta K_{rr'}(\mathbf{p}-\mathbf{p}')\delta''(\varepsilon_{r'p'}-\varepsilon_{rp}),$$

$$\Delta W_{r\mathbf{p}r'\mathbf{p}'}=\Delta K_{rr'}(\mathbf{p}-\mathbf{p}')\delta(\varepsilon_{r'p'}-\varepsilon_{rp}). \tag{4}$$

Here $\delta'(E)$ and $\delta''(E)$ are the first and second derivatives of the δ function and the kernels $K_{rr'}$ and $\Delta K_{rr'}$ are given by

$$K_{rr'}(\mathbf{p}-\mathbf{p}')=\frac{4\pi}{\hbar}\sum_{\mathbf{Q}}|C_Q^{(\rm ac)}|^2\left|\langle r'\mathbf{p}'|\,e^{i\mathbf{Q}r}\,|r\mathbf{p}\rangle\right|^2\frac{T_{\rm ph}}{\hbar\omega_Q},$$

$$\Delta K_{rr'}(\mathbf{p}-\mathbf{p}')=\frac{4\pi}{\hbar}\sum_{\mathbf{Q}}|C_Q^{(\rm ac)}|^2|\langle r'\mathbf{p}'|\,e^{i\mathbf{Q}r}\,|r\mathbf{p}\rangle|^2\hbar\omega_Q, \tag{5}$$

where $C_Q^{(\rm ac)}$ is the bulk matrix element for the deformation interaction.

We restrict ourselves to the sequential tunneling processes under the condition $T\ll\varepsilon_B$. Considering only the proportional to $(T/\varepsilon_B)^2$ corrections to the overlap factors, we use

$$\left|\langle r'\mathbf{p}'|\,e^{i\mathbf{Q}r}\,|r\mathbf{p}\rangle\right|^2\simeq\delta_{\mathbf{p}'\mathbf{p}+\hbar\mathbf{q}}\Psi_{q_\perp d}\left[\delta_{rr'}+\left(\frac{T}{\varepsilon_B}\right)^2(\delta_{rr'+1}+\delta_{rr'-1})\right], \tag{6}$$

where $\mathbf{Q}=(\mathbf{q},q_\perp)$ is written through the in-plane, $\mathbf{q}$, and transverse, $q_\perp$, components of the wave vector and $\Psi_{q_\perp d}=|\langle 0|e^{iq_\perp z}|0\rangle|^2$ describes the transverse overlap between the ground states of the QWs, $|0\rangle$. Since all QWs are identical and $\varepsilon_{r'p'}-\varepsilon_{rp}=(r-r')\varepsilon_B+\varepsilon_{p'}-\varepsilon_p$, the distribution functions are the same in any QW, i.e., $f_{r\mathbf{p}}\to f_{\mathbf{p}}$. Thus, the collision integrals in Eqs. (2) and (3) are independent of r because the summation over r' is replaced by $\Sigma_{\Delta r=\pm 1}\cdots$. The collision integral in Eq. (2) is transformed into

$$J_{\rm LO}(f|\mathbf{p})\simeq\frac{2\pi}{\hbar}\sum_{r'\mathbf{p}'q_\perp}|C_Q^{(\rm LO)}|^2\Psi_{q_\perp d}\times\left\{\delta(\varepsilon_{p'}-\varepsilon_p-\hbar\omega_0)f_{\mathbf{p}'}-\delta(\varepsilon_p-\varepsilon_{p'}-\hbar\omega_0)f_{\mathbf{p}}+\left(\frac{T}{\varepsilon_B}\right)^2\sum_{\Delta r=\pm 1}[\delta(\Delta r\varepsilon_B+\varepsilon_{p'}-\varepsilon_p-\hbar\omega_0)f_{\mathbf{p}'}-\delta(\Delta r\varepsilon_B+\varepsilon_{p'}-\varepsilon_p+\hbar\omega_0)f_{\mathbf{p}}]\right\}, \tag{7}$$

where $\Sigma_{\Delta r=\pm 1}\cdots$ describes the interwell tunneling with LO-phonon emission and $Q^2=|\mathbf{p}-\mathbf{p}'|^2/\hbar^2+q_\perp^2$.

Below we restrict ourselves to the thin QW case when $|C_Q^{(\mathrm{ac})}|^2$ can be replaced by $|C_{q_\perp}^{(\mathrm{ac})}|^2$. Similar transformations for the acoustic phonon contribution of Eq. (3) give us[13,14]

$$J_{\mathrm{ac}}(f|\mathbf{p}) = K_{\mathrm{ac}}\sum_{\mathbf{p}'}\left[\delta(\varepsilon_{p'}-\varepsilon_p)+\sum_{\Delta r=\pm 1}\left(\frac{T}{\varepsilon_B}\right)^2\delta(\Delta r\varepsilon_B+\varepsilon_{p'}-\varepsilon_p)\right](f_{\mathbf{p}'}-f_{\mathbf{p}}) - \Delta K\sum_{\mathbf{p}'}\frac{T_{\mathrm{ph}}}{2}\delta'(\varepsilon_{p'}-\varepsilon_p)(f_{\mathbf{p}'}-f_{\mathbf{p}}) - \frac{1}{2}\delta'(\varepsilon_{p'}-\varepsilon_p)(f_{\mathbf{p}'}+f_{\mathbf{p}}). \tag{8}$$

Here we have neglected weak ($\propto\Delta K$) contributions to the tunneling transitions. The kernels in Eq. (5) appear to be momentum independent,

$$K_{\mathrm{ac}} \approx \frac{4\pi}{\hbar}\sum_{q_\perp}|C_{q_\perp}^{(\mathrm{ac})}|^2\Psi_{q_\perp d}\frac{T_{\mathrm{ph}}}{\hbar\omega_{q_\perp}},$$

$$\Delta K \approx \frac{4\pi}{\hbar}\sum_{q_\perp}|C_{q_\perp}^{(\mathrm{ac})}|^2\Psi_{q_\perp d}\hbar\omega_{q_\perp}, \tag{9}$$

due to the narrow QW approximation. The intrawell and interwell scatterings caused by the static disorder can be described in a similar way to the elastic ($\propto K_{\mathrm{ac}}$) contributions in Eq. (8),

$$J_d(f|\mathbf{p}) = K_d\sum_{\mathbf{p}'}\left[\delta(\varepsilon_{p'}-\varepsilon_p)+\sum_{\mathbf{p}'\Delta r=\pm 1}\left(\frac{T}{\varepsilon_B}\right)^2\delta(\Delta r\varepsilon_B+\varepsilon_{p'}-\varepsilon_p)\right](f_{\mathbf{p}'}-f_{\mathbf{p}}). \tag{10}$$

Factors K_d and K_{ac} determine the departure relaxation rates caused by the elastic scattering mechanisms as $\nu_{d,\mathrm{ac}}=K_{d,\mathrm{ac}}\Sigma_{\mathbf{p}'}\delta(\varepsilon_{p'}-\varepsilon_p)\propto\rho_{2\mathrm{D}}$, where $\rho_{2\mathrm{D}}$ is the 2D density of states.

B. Nonequilibrium distribution

We search for the solution of Eq. (1) in the form $f_{\mathbf{p}}\simeq f_\varepsilon+\Delta f_{\mathbf{p}}$, where f_ε describes the lateral heating due to tunneling current and $\Delta f_{\mathbf{p}}$ is the in-plane anisotropic addendum due to the weak field $\mathbf{E}$. We consider the symmetric part of the distribution which is governed by the kinetic equation $\Sigma_k J_k(f|\varepsilon)=0$ and satisfies the normalization condition

$$nZ=\rho_{2\mathrm{D}}\int_0^\infty d\varepsilon f_\varepsilon \tag{11}$$

with the layer concentration nZ. Averaging Eq. (7) over $\mathbf{p}$ plane and taking into account the energy conservation condition, one obtains the LO contribution as a finite-difference form,

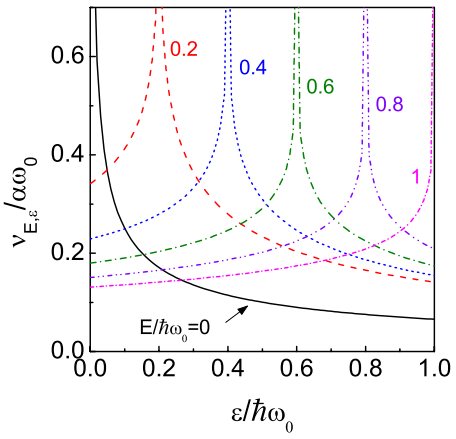

FIG. 2. (Color online) Dimensionless relaxation rate $\nu_{E,\varepsilon}/\alpha\omega_0$ versus $\varepsilon/\hbar\omega_0$ plotted in the passive region for $E/\hbar\omega_0=0$, 0.2, 0.4, 0.6, 0.8, and 1.

$$J_{\mathrm{LO}}(f|\varepsilon) = \nu_{\varepsilon+\hbar\omega_0,\varepsilon}f_{\varepsilon+\hbar\omega_0}-\nu_{\varepsilon-\hbar\omega_0,\varepsilon}f_\varepsilon + \sum_{\Delta r=\pm 1}[\nu^t_{\varepsilon+\hbar\omega_0-\Delta r\varepsilon_B,\varepsilon}f_{\varepsilon+\hbar\omega_0-\Delta r\varepsilon_B}-\nu^t_{\varepsilon-\hbar\omega_0-\Delta r\varepsilon_B,\varepsilon}f_\varepsilon]. \tag{12}$$

Here the tunneling contributions $\nu^t_{E,\varepsilon}=(T/\varepsilon_B)^2\nu_{E,\varepsilon}$ are reduced by the factor $(T/\varepsilon_B)^2$. We introduce the relaxation rate describing the spontaneous emission of LO phonons as follows:

$$\nu_{E,\varepsilon}=\frac{2\pi}{\hbar}\sum_{\mathbf{p}'q_\perp}|C_Q^{(\mathrm{LO})}|^2\Psi_{q_\perp d}\delta(\varepsilon_{p'}-E). \tag{13}$$

Performing the integration over $\mathbf{p}'$ plane one obtains

$$\nu_{E,\varepsilon}=\theta(E)\alpha\omega_0\int_{-\infty}^{\infty}dx\Psi_x\sqrt{\frac{\varepsilon_d\hbar\omega_0}{(\varepsilon_d x^2+\varepsilon+E)^2-4\varepsilon E}}, \tag{14}$$

where α is the polaron coupling constant and $\varepsilon_d=(\hbar/d)^2/2m$. This rate is on the order of $\alpha\omega_0$. Figure 2 shows the dimensionless relaxation rate $\nu_{E,\varepsilon}/\alpha\omega_0$ versus $\varepsilon/\hbar\omega_0$, plotted in the passive region for different $E/\hbar\omega_0$ values and for a 60-Å-wide QW, when $\varepsilon_d/\hbar\omega_0\simeq 0.44$. Note that $\nu_{E,\varepsilon}$ appears to be logarithmically divergent if $E\to\varepsilon$.

The intrawell process of quasielastic energy relaxation is described by the Fokker-Planck collision integral[13] given by

$$J_{\mathrm{ac}}(f|\varepsilon)\approx\nu_{\mathrm{ac}}\bar{\varepsilon}^2\frac{d}{d\varepsilon}\left(\frac{df_\varepsilon}{d\varepsilon}+\frac{f_\varepsilon}{T_{\mathrm{ph}}}\right), \tag{15}$$

where ν_{ac} is the above-introduced departure relaxation rate and $\bar{\varepsilon}^2\simeq(\Delta K/K_{\mathrm{ac}})T_{\mathrm{ph}}/2$. The elastic tunneling relaxation caused by disorder and acoustic phonons [see Eqs. (8) and (10)] is governed by the finite-difference contribution

$$J_t(f|\varepsilon)\simeq\nu_t\sum_{\Delta r=\pm 1}\theta(\varepsilon-\Delta r\varepsilon_B)(f_{\varepsilon-\Delta r\varepsilon_B}-f_\varepsilon) \tag{16}$$

with the tunneling rate $\nu_t=(T/\varepsilon_B)^2(\nu_d+\nu_{\mathrm{ac}})$. Thus, the distribution f_ε is governed by the equation

$$J_{\rm ac}(f|\varepsilon) + J_t(f|\varepsilon) + J_{\rm LO}(f|\varepsilon) = 0. \quad (17)$$

Moreover, in the active region, $\varepsilon > \hbar\omega_0$, the main contribution is due to the spontaneous emission of LO phonons [first and second terms of Eq. (12)].

In the active region, $\varepsilon > \hbar\omega_0$, the distribution decreases fast. Thus, in the kinetic equation, one has to take into account the second derivative from Eq. (15) and the spontaneous emission contribution from Eq. (12),

$$\nu_{\rm ac}\bar{\varepsilon}^2 \frac{d^2 f_\varepsilon}{d\varepsilon^2} - \nu_{\rm LO} f_\varepsilon = 0, \quad (18)$$

where $\nu_{\rm LO} = \nu_{0,\hbar\omega_0}$. Using the boundary condition $f_{\varepsilon\to\infty} = 0$ one obtains the solution $f_\varepsilon \approx f_{\hbar\omega_0} \exp[-\lambda_0(\varepsilon - \hbar\omega_0)]$ with $\lambda_0 = \sqrt{\nu_{\rm LO}/\nu_{\rm ac}}\bar{\varepsilon}^{-1}$.

Next, eliminating the fast spontaneous emission of LO phonons one obtains Eq. (17) in the passive region with the boundary condition

$$\left(\frac{d}{d\varepsilon} + \lambda_0\right) f_{\varepsilon\to\hbar\omega_0 - 0} = 0. \quad (19)$$

Thus, the problem formulated in the passive region takes into account the quasielastic energy relaxation described by Eq. (15) and the interwell tunneling transitions shown in Figs. 1(b)–1(d). The normalization condition should be restricted over the passive region and Eq. (11) is transformed into $nZ = \rho_{\rm 2D}\int_0^{\hbar\omega_0} d\varepsilon f_\varepsilon$.

C. Lateral conductivity

Further, we turn to the description of the linear response given by $\Delta f_{\mathbf{p}} \propto \mathbf{E}$ and consider the current density

$$\mathbf{I} = \frac{2e}{Zm}\int \frac{d\mathbf{p}}{(2\pi\hbar)^2}\mathbf{p}\Delta f_{\mathbf{p}}. \quad (20)$$

The nonsymmetric part of the distribution function $\Delta f_{\mathbf{p}}$ is determined from the linearized kinetic equation

$$e\mathbf{E}\cdot\frac{\partial f_\varepsilon}{\partial \mathbf{p}} = \sum_k J_k(\Delta f|\mathbf{p}), \quad (21)$$

where the elastic collision integrals due to ac and d contributions can be replaced by $-\nu_m \Delta f_{\mathbf{p}}$. Here $\nu_m = \nu_d + \nu_{\rm ac}$ is the momentum relaxation rate due to the elastic scattering [see Eqs. (8) and (10)]. The nonelastic momentum relaxation due to the optical-phonon-induced interwell transitions, $J_{\rm LO}(\Delta f|\mathbf{p})$, is given by the $\propto (T/\varepsilon_B)^2$ contribution of Eq. (7). Introducing the energy-dependent function χ_ε according to $\Delta f_{\mathbf{p}} = (e/m)(\mathbf{E}\cdot\mathbf{p})\chi_\varepsilon$, we transform Eq. (21) into the finite-difference equation,

$$\frac{df_\varepsilon}{d\varepsilon} = -\nu_m\chi_\varepsilon + \sum_{\Delta r=\pm 1}[\tilde{\nu}^t_{\varepsilon+\hbar\omega_0-\Delta r\varepsilon_B,\varepsilon}\chi_{\varepsilon+\hbar\omega_0-\Delta r\varepsilon_B} - \nu^t_{\varepsilon-\hbar\omega_0-\Delta r\varepsilon_B,\varepsilon}\chi_\varepsilon]. \quad (22)$$

Here $\tilde{\nu}^t_{E,\varepsilon} = (T/\varepsilon_B)^2\tilde{\nu}_{E,\varepsilon}$ is the tunneling-induced relaxation rate where

$$\tilde{\nu}_{E,\varepsilon} = \frac{2\pi}{\hbar}\sum_{\mathbf{p}'q_\perp} |C_Q^{\rm (LO)}|^2 \Psi_{q_\perp d}\cos(\hat{\mathbf{p},\mathbf{p}'})\delta(\varepsilon - \varepsilon_{p'} - E), \quad (23)$$

which uses a similar notation to Eq. (13).

Introducing the in-plane conductivity, σ, according to $\mathbf{I} = \sigma\mathbf{E}$ we obtain

$$\sigma = \frac{e^2\rho_{\rm 2D}}{mZ}\int_0^{\hbar\omega_0} d\varepsilon\varepsilon\chi_\varepsilon. \quad (24)$$

Here we neglect the contribution from $\varepsilon > \hbar\omega_0$ because of the smallness of $\chi_\varepsilon \simeq \nu_{\rm LO}^{-1}(-df_\varepsilon/d\varepsilon)$ in the active region. Under the condition $\nu_m \gg \nu^t_{\rm LO}$ Eq. (22) gives $\chi_\varepsilon \simeq \nu_m^{-1}(-df_\varepsilon/d\varepsilon)$ and the conductivity takes the form

$$\sigma = \sigma_0\left(1 - \frac{\rho_{\rm 2D}\hbar\omega_0}{n_{\rm 2D}}f_{\hbar\omega_0}\right), \quad \sigma_0 = \frac{e^2 n_{\rm 2D}}{m\nu_m Z}. \quad (25)$$

As a result, σ/σ_0 is expressed through the distribution function at $\varepsilon = \hbar\omega_0$ and a negative lateral conductivity takes place at $f_{\hbar\omega_0} > n_{\rm 2D}/\rho_{\rm 2D}\hbar\omega_0$.

III. SECOND-ORDER BLOCH-PHONON RESONANCE

Before analyzing the general problem, we consider the simple resonant case $2\varepsilon_B = \hbar\omega_0$ when the distribution can be considered over two intervals: $0 < \varepsilon < \hbar\omega_0/2$ and $\hbar\omega_0/2 < \varepsilon < \hbar\omega_0$. Introducing the functions over the interval $0 < \varepsilon < \hbar\omega_0/2$ according to $f_{1\varepsilon} = f_\varepsilon$ and $f_{2\varepsilon} = f_{\varepsilon+\hbar\omega_0}$, we transform Eq. (17) [or Eqs. (A1) and (A3) in Appendix] into the system

$$J_{\rm ac}(f_1|\varepsilon) + \nu_t(2f_{2\varepsilon} - f_{1\varepsilon}) + \nu^t_{\varepsilon+\hbar\omega_{0/2},\varepsilon}f_{2\varepsilon} = 0,$$

$$J_{\rm ac}(f_2|\varepsilon) + \nu_t(f_{1\varepsilon} - 2f_{2\varepsilon}) - \nu^t_{\varepsilon,\varepsilon+\hbar\omega_{0/2}}f_{2\varepsilon} = 0. \quad (26)$$

Here $\nu_t \simeq (T/\varepsilon_B)^2\nu_m$ is the elastic tunneling rate and $\nu^t_{E,\varepsilon}$ was introduced in Eq. (12). The two second-order differential equations in Eq. (26) should be solved with the boundary condition of Eq. (19), the normalization condition $nZ = \rho_{\rm 2D}\int_0^{\hbar\omega_{0/2}} d\varepsilon(f_{1\varepsilon} + f_{2\varepsilon})$, as well as the inhomogeneous conditions $f_{1\hbar\omega_{0/2}} = f_{2\varepsilon=0}$ and $(df_{1\varepsilon}/d\varepsilon)_{\hbar\omega_{0/2}} = (df_{2\varepsilon}/d\varepsilon)_0$.

Figure 3 shows the distribution function f_ε versus in-plane kinetic energy obtained from system (26) for different $T_{\rm ph}$, T, and ν_m. As can be seen, peaks of f_ε widen as temperature increases, reducing their maxima. The effect of interwell coupling $\propto T$ and elastic scattering $\propto \nu_m$ is also evident, founding that peaks increase as these parameters do. Calculations have been made for a concentration $n_{\rm 2D} = 10^9$ cm^{-2} (or $n = 10^{15}$ cm^{-3} if $Z = 100$ Å), so that $f_{1\varepsilon} \leq 0.1$ and electrons are nondegenerate.[15] For this value, $n_{\rm 2D}/\rho_{\rm 2D}\hbar\omega_0 \sim 10^{-3}$. Peaks located at $\hbar\omega_0/2$ and $\hbar\omega_0$ are on the order of 10^{-2} and 10^{-3}, respectively. Therefore, the last value is big enough to obtain ANC because of $f_{\hbar\omega_0} > n_{\rm 2D}/\rho_{\rm 2D}\hbar\omega_0$, according to Eq. (25). In order to magnify peaks at $\varepsilon/\hbar\omega_0 = 0.5$ and 1, we have limited vertical axis size.

Figure 4 describes normalized lateral conductivity σ/σ_0 given by Eq. (25) vs momentum relaxation rate ν_m, for temperatures $T_{\rm ph} = 4.2$ and 20 K, and tunneling coupling $T = 5$

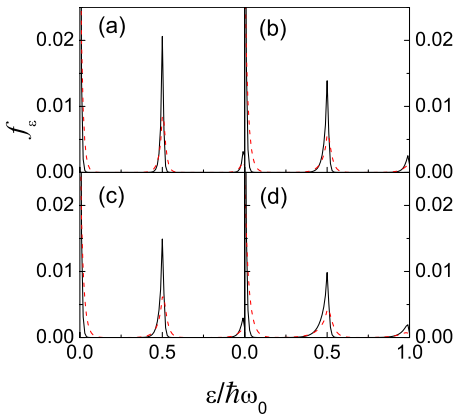

FIG. 3. (Color online) Distribution function f_ε vs in-plane kinetic energy obtained from system (26) at $T_{\rm ph}=4.2$ and 20 K (solid and dashed curves) for (a) $T=5$ meV and $\nu_m=1$ ps^{-1}, (b) $T=5$ meV and $\nu_m=0.5$ ps^{-1}, (c) $T=3.5$ meV and $\nu_m=1$ ps^{-1}, and (d) $T=3.5$ meV and $\nu_m=0.5$ ps^{-1}.

and 3.5 meV. Because of the distribution function peaks at $\hbar\omega_0$ increase as T and ν_m do (see Fig. 3), lateral conductivity decreases correspondingly leading to negative values for a wide region of parameters. As we saw in Fig. 3, the effect of the temperature is opposed to the previous ones. For high temperatures σ increases to reach σ_0 and the possibility of having ANC disappears.

IV. NUMERICAL RESULTS

We turn now to the numerical calculations of the nonequilibrium distribution f_ε governed by Eq. (17), with the boundary condition defined by Eq. (19), and the normalization requirement [the explicit form of Eq. (17) for the cases $\varepsilon_B<\hbar\omega_0/2$, $\hbar\omega_0/2<\varepsilon_B<\hbar\omega_0$, and $\hbar\omega_0<\varepsilon_B$ are given in Appendix]. We also analyze the lateral conductivity solving the finite-difference Eq. (22) [see explicit expressions (A2),

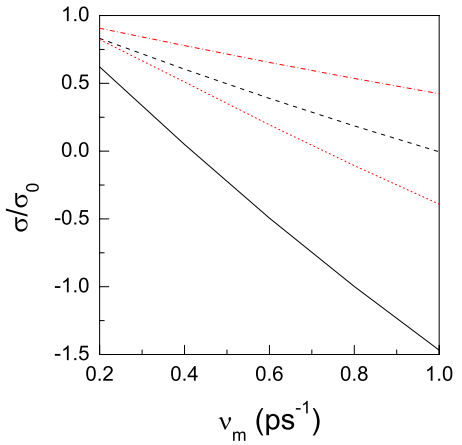

FIG. 4. (Color online) Normalized conductivity σ/σ_0, given by Eq. (25), vs momentum relaxation rate ν_m for different temperatures and tunneling coupling values ($T_{\rm ph}$ and T). Solid line: 4.2 K and 5 meV. Dashed line: 20 K and 5 meV. Dotted line: 4.2 K and 3.5 meV. Dashed-dotted line: 20 K and 3.5 meV.

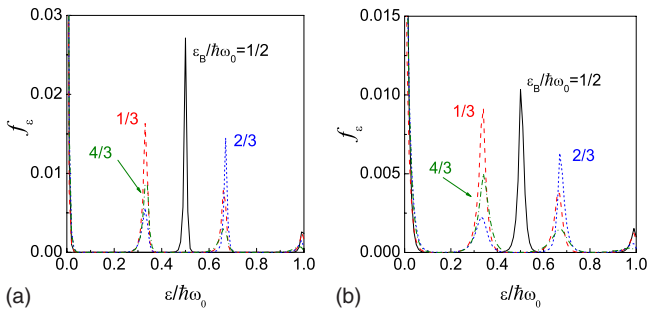

FIG. 5. (Color online) Distribution function f_ε vs in-plane kinetic energy for different $\varepsilon_B/\hbar\omega_0$ values (1/3, 1/2, 2/3, and 4/3) in GaAs/$Al_{0.3}Ga_{0.7}$As-based BSL at different temperatures: (a) $T_{\rm ph}=4.2$ K and (b) $T_{\rm ph}=20$ K.

(A4), and (A6)] and performing the integration in Eq. (24). Calculations below are performed for the GaAs/$Al_{0.3}Ga_{0.7}$As-based SL, formed by 60-Å-wide QWs separated by barriers of 32 Å (or 37 Å) wide, which correspond to the tunneling matrix element $T=5$ meV (or 3.5 meV). We have chosen this structure because it has only a miniband inside the wells around 65 meV. We consider temperatures of $T_{\rm ph}=4.2$ and 20 K as well as the effect of the elastic scattering variation through the momentum relaxation rate $\nu_m=1$ and 0.5 ps^{-1}. It is convenient to use $n_{2D}=10^9$ cm^{-2} in spite of σ/σ_0 does not depend on concentration.

Figure 5 displays the distribution function f_ε vs the in-plane kinetic energy for different $\varepsilon_B/\hbar\omega_0$ values (1/3, 1/2, 2/3, and 4/3) obtained from general Eq. (17) (see also Appendix). When comparing the case $\varepsilon_B/\hbar\omega_0=1/2$ of Figs. 5(a) and 5(b) with the panel (a) in Fig. 3, calculated in Sec. III for the same parameters, a good agreement is found. As mentioned before, temperature effect is reflected as a widening and decreasing of the peaks. For other N/M values f_ε shows lower relative maxima.

Next we calculate the normalized lateral conductivity solving Eq. (22) and using f_ε obtained before. Figure 6 represents σ/σ_0 as a function of the Bloch energy $\varepsilon_B/\hbar\omega_0$ and for different temperature, elastic scattering, and tunneling coupling values. General behavior shows a pronounced relative minimum located at $\varepsilon_B/\hbar\omega_0=1$, followed by other relative minima at 1/2, 1/3, 2/3, 1/4,… (in decreasing order). In the active region, when $N>M$, these peaks are practically negligible. Depending on parameters some of the peaks reach negative values. A detailed quantitative description can be seen through Table I, where we have included the minimum values (σ_m/σ_0) and the half with at half maximum (minimum in this case, HWHM) of the relative transverse conductivity for the main peaks of Fig. 6. Thus, (a)–(d) in the table correspond to panels (a)–(d) in Fig. 6. Looking through the columns of the table it can be seen, for every case, that minima are more pronounced for $\varepsilon_B/\hbar\omega_0=1$ and decrease following the series (from bigger to smaller) 1, 1/2, 1/3, 2/3 (1/4, 3/4,…). As an example, size of the peaks decreases around a 50% from $\varepsilon_B/\hbar\omega_0=1$ to $\varepsilon_B/\hbar\omega_0=1/2$ and around a 33% from $\varepsilon_B/\hbar\omega_0=1/2$ to $\varepsilon_B/\hbar\omega_0=1/3$. On the other hand, the HWHM of the peaks diminishes nonmonotonically as $\varepsilon_B/\hbar\omega_0$ do.

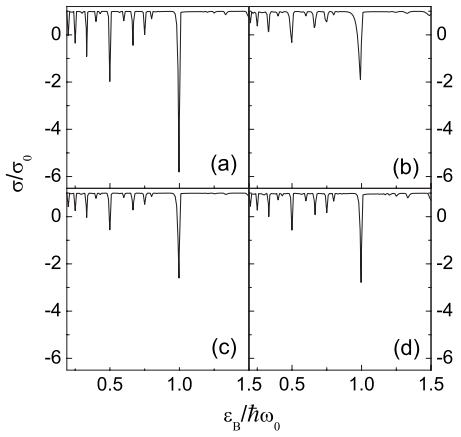

FIG. 6. Normalized lateral conductivity vs Bloch energy $\varepsilon_B/\hbar\omega_0$ and for different temperature, elastic scattering, and tunneling coupling ($T_{\rm ph}$, ν_m, and T). (a) 4.2 K, 1 ps^{-1}, and 5 meV. (b) 20 K, 1 ps^{-1}, and 5 meV. (c) 4.2 K, 1 ps^{-1}, and 3.5 meV. (d) 4.2 K, 0.5 ps^{-1}, and 5 meV.

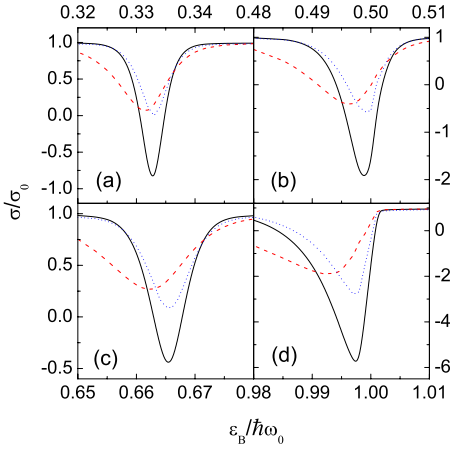

FIG. 7. (Color online) Normalized conductivity vs Bloch energy $\varepsilon_B/\hbar\omega_0$ around (a) 1/3, (b) 1/2, (c) 2/3, and (d) 1 for T=5 meV. Solid lines: ν_m=1 ps^{-1} and $T_{\rm ph}$=4.2 K. Dashed lines: ν_m=1 ps^{-1} and $T_{\rm ph}$=20 K. Dotted lines: ν_m=0.5 ps^{-1} and $T_{\rm ph}$=4.2 K.

To clarify the effect of the different parameters we can compare in pairs the panels in Fig. 6. Thus, comparing panels (a) and (b) we can see the temperature effect, which is similar to the one found before for the distribution function: peaks are wider and less pronounced when temperature increases, leading to less negative values. Looking at the columns labeled (a) and (b) in the table, we can see that, when increasing temperature from $T_{\rm ph}$=4.2 K until $T_{\rm ph}$=20 K, the peaks get around 60% wider and around 50% smaller. Comparing panels (a) and (c) in Fig. 6, the effect of the tunneling coupling can be visible: if T decreases from 5 to 3.5 meV (increasing barriers' width) size of peak minima is reduced. From columns (a) and (c) in the table we get a reduction of about 50%. However, HWHM is practically insensitive to the variation in T, showing only a slight spread. Finally, an analogous behavior is observed comparing panels (a) and (d) to see the elastic scattering effect. Reducing ν_m from 1 to 0.5 ps^{-1} we obtain a decreasing in the peaks in a similar way around 45%. The HWHM of the conductivity peaks is even more insensitive to this parameter than in the previous case. One can conclude that the most favorable conditions to get negative conductivity correspond to low temperature and big tunneling coupling and elastic scattering values.

TABLE I. Minimum values and HWHM of relative transverse conductivity for the main peaks of Fig. 6.

$\varepsilon_B/\hbar\omega_0$	σ_m/σ_0 (a)	HWHM (a)	σ_m/σ_0 (b)	HWHM (b)
1	−5.75	0.0078	−1.911	0.0206
1/2	−1.93	0.006	−0.416	0.0135
1/3	−0.83	0.005	0.064	0.0098
2/3	−0.44	0.007	0.266	0.0165
$\varepsilon_B/\hbar\omega_0$	σ_m/σ_0 (c)	HWHM (c)	σ_m/σ_0 (d)	HWHM (d)
1	−2.6	0.0081	−2.8	0.0085
1/2	−0.56	0.0067	−0.58	0.0068
1/3	−0.05	0.0055	−0.0013	0.0056
2/3	0.28	0.0076	0.08	0.0072

In order to detail the shape of the normalized conductivity peaks we present some of them in Fig. 7. We have chosen the more noticeable ones, corresponding to Bloch energy $\varepsilon_B/\hbar\omega_0$ around 1/3 [panel (a)], 1/2 (b), 2/3 (c), and 1 (d), for T=5 meV, with temperature and elastic scattering values corresponding to panels (a), (b), and (d) included in Fig. 6. A breakdown of the peak symmetry is observable when $\varepsilon_B/\hbar\omega_0$ increases going from a quite symmetric peak for $\varepsilon_B/\hbar\omega_0$ close to 1/3 to a clearly asymmetric peak around 1.

V. CONCLUDING REMARKS

In summary, we have demonstrated that the negative lateral conductivity regime is possible in low-doped biased superlattices under the Bloch-phonon resonance conditions. When analyzing the dependence of σ vs bias voltage, narrow negative peaks take place if $\varepsilon_B/\hbar\omega_0$ is close to the ratio 1/2, 1/3, 2/3,…. ANC regime appears to be most pronounced for low-temperature region in BSL with an effective interwell coupling.

Next, we list the assumptions used. The main restriction of the ANC regime is neglecting the electron-electron scattering, imposed by the Maxwell distribution, with an effective temperature suppressing the high-energy part of the distribution. The condition $\sigma<0$ does not depend on concentration for nondegenerate electrons. Thus, we have used in the calculations $n_{2D}<10^{10}$ cm^{-2}, where the electron-electron scattering is not the main scattering process (see Ref. 16, where different systems were considered). The evaluation of the limiting concentration, which requires to involve the electron-electron collision integral in Eq. (17), lies beyond the scope of this paper. Another approximation we have made is rather standard. In order to estimate the coefficients of the kinetic equation, we have used a tight-binding approach for the description of the electronic states.[8] We consider the narrow QW case when SL is formed due to tunnel coupling of the ground states while the excited states

are omitted. The use of the bulk model for phonon dispersion and electron-phonon interaction is a reasonable approximation for the GaAs/AlGaAs-based structures.[17] The quasielastic scattering by acoustic phonons is described with the expansion of the energy conserving delta function in Eq. (3), which is valid if $\hbar\omega_Q$ is less than electron energy. Since $\omega_Q = sQ$ with a slow sound velocity s, the above condition is valid for the case under consideration. As phonon temperature increases, the negative conductivity is suppressed, so that an effective cooling of the acoustic phonon thermostat is a necessary condition. We consider the momentum relaxation due to short-range scattering neglecting a large-scale potential; last contributions require a special attention in analogy with the case of a single low-doped well. We restrict ourselves to the case of uniform bias fields and equipopulated wells neglecting the possible domain formation [one can avoid instabilities of vertical current in a short enough BSL (Ref. 18)].

We should mention also that an experimental task for measuring the lateral conductivity of BSL is not simple because a complicate contribution of the corner regions is possible. But, instead of the dc measurements, one can use a high-frequency contactless study of the response using a transverse capacitor. In addition, under the instability conditions (if $\sigma<0$) a direct measurement of lateral conductivity is not necessary because the vertical current appears to be unstable. A detailed description of this unstable response requires a special consideration.

To conclude, a low-doped BSL at low temperature is a suitable structure in order to realize the absolute negative conductivity regime. In addition, a similar behavior is possible not only for the BSL under consideration but also for the more complicated tunnel-coupled structure used in quantum cascade lasers. An instability of such a structure for the case of low doping and temperature is possible and should be checked additionally.

APPENDIX: KINETIC EQUATIONS

Below we rewrite Eqs. (17) and (22) for cases (A) $\varepsilon_B < \hbar\omega_0/2$, (B) $\hbar\omega_0/2 < \varepsilon_B < \hbar\omega_0$, and (C) $\hbar\omega_0 < \varepsilon_B$.

For case A, when $\varepsilon_B < \hbar\omega_0 - \varepsilon_B < \hbar\omega_0$ [see Fig. 1(b)], the distribution in the passive region f_ε is described by the system

$$J_{\rm ac}(f|\varepsilon) + \nu_t(f_{\varepsilon+\varepsilon_B} + f_{\varepsilon+\hbar\omega_0-\varepsilon_B} - f_\varepsilon) + \nu^t_{\varepsilon+\hbar\omega_0-\varepsilon_B,\varepsilon} f_{\varepsilon+\hbar\omega_0-\varepsilon_B} = 0, \quad 0 < \varepsilon < \varepsilon_B,$$

$$J_{\rm ac}(f|\varepsilon) + \nu_t(f_{\varepsilon+\varepsilon_B} + f_{\varepsilon+-\varepsilon_B} - 2f_\varepsilon) = 0, \quad \varepsilon_B < \varepsilon < \hbar\omega_0 - \varepsilon_B,$$

$$J_{\rm ac}(f|\varepsilon) + \nu_t(f_{\varepsilon-\varepsilon_B} - 2f_\varepsilon) - \nu^t_{\varepsilon-\hbar\omega_0+\varepsilon_B,\varepsilon} f_\varepsilon = 0, \quad \hbar\omega_0 - \varepsilon_B < \varepsilon < \hbar\omega_0, \tag{A1}$$

which is written for the three intervals $0<\varepsilon<\varepsilon_B$, $\varepsilon_B<\varepsilon<\hbar\omega_0-\varepsilon_B$, and $\hbar\omega_0-\varepsilon_B<\varepsilon<\hbar\omega_0$. Equation (22) in this case is transformed into the system

$$\frac{df_\varepsilon}{d\varepsilon} = -\nu_m\chi_\varepsilon + \tilde{\nu}^t_{\varepsilon+\hbar\omega_0-\varepsilon_B,\varepsilon}\chi_{\varepsilon+\hbar\omega_0-\varepsilon_B}, \quad 0 < \varepsilon < \varepsilon_B,$$

$$\frac{df_\varepsilon}{d\varepsilon} = -\nu_m\chi_\varepsilon, \quad \varepsilon_B < \varepsilon < \hbar\omega_0 - \varepsilon_B,$$

$$\frac{df_\varepsilon}{d\varepsilon} = -(\nu_m + \nu^t_{\varepsilon-\hbar\omega_0+\varepsilon_B,\varepsilon})\chi_\varepsilon, \quad \hbar\omega_0 - \varepsilon_B < \varepsilon < \hbar\omega_0. \tag{A2}$$

In case B, when $\hbar\omega_0-\varepsilon_B<\varepsilon_B<\hbar\omega_0$ [see Fig. 1(c)], Eq. (17) is transformed into the system

$$J_{\rm ac}(f|\varepsilon) + \nu_t(f_{\varepsilon+\varepsilon_B} + f_{\varepsilon+\hbar\omega_0-\varepsilon_B} - f_\varepsilon) + \nu^t_{\varepsilon+\hbar\omega_0-\varepsilon_B,\varepsilon} f_{\varepsilon+\hbar\omega_0-\varepsilon_B} = 0, \quad 0 < \varepsilon < \hbar\omega_0 - \varepsilon_B,$$

$$J_{\rm ac}(f|\varepsilon) + \nu_t(f_{\varepsilon+\hbar\omega_0-\varepsilon_B} - f_\varepsilon) + \nu^t_{\varepsilon+\hbar\omega_0-\varepsilon_B,\varepsilon} f_{\varepsilon+\hbar\omega_0-\varepsilon_B} - \nu^t_{\varepsilon-\hbar\omega_0+\varepsilon_B,\varepsilon} f_\varepsilon = 0, \quad \hbar\omega_0 - \varepsilon_B < \varepsilon < \varepsilon_B,$$

$$J_{\rm ac}(f|\varepsilon) + \nu_t(f_{\varepsilon-\varepsilon_B} - 2f_\varepsilon) - \nu^t_{\varepsilon-\hbar\omega_0+\varepsilon_B,\varepsilon} f_\varepsilon = 0, \quad \varepsilon_B < \varepsilon < \hbar\omega_0. \tag{A3}$$

while Eq. (22) takes the form

$$\frac{df_\varepsilon}{d\varepsilon} = -\nu_m\chi_\varepsilon + \tilde{\nu}_{\varepsilon+\hbar\omega_0-\varepsilon_B,\varepsilon}\chi_{\varepsilon+\hbar\omega_0-\varepsilon_B}, \quad 0 < \varepsilon < \hbar\omega_0 - \varepsilon_B,$$

$$\frac{df_\varepsilon}{d\varepsilon} = -(\nu_m + \nu^t_{\varepsilon-\hbar\omega_0+\varepsilon_B,\varepsilon})\chi_\varepsilon + \tilde{\nu}_{\varepsilon+\hbar\omega_0-\varepsilon_B,\varepsilon}\chi_{\varepsilon+\hbar\omega_0-\varepsilon_B}, \quad \hbar\omega_0 - \varepsilon_B < \varepsilon < \varepsilon_B,$$

$$\frac{df_\varepsilon}{d\varepsilon} = -(\nu_m + \tilde{\nu}_{\varepsilon-\hbar\omega_0+\varepsilon_B,\varepsilon})\chi_\varepsilon, \quad \varepsilon_B < \varepsilon < \hbar\omega_0. \tag{A4}$$

Similarly, for high-biased SL [case C when $\hbar\omega_0<\varepsilon_B$, see Fig. 1(d)] one obtains the system

$$J_{\rm ac}(f|\varepsilon) + \nu^t_{\varepsilon+2\hbar\omega_0-\varepsilon_B,\varepsilon} f_{\varepsilon+2\hbar\omega_0-\varepsilon_B} - \nu^t_{\varepsilon-\hbar\omega_0+\varepsilon_B,\varepsilon} f_\varepsilon = 0, \quad 0 < \varepsilon < \varepsilon_B - \hbar\omega_0,$$

$$J_{\rm ac}(f|\varepsilon) + \nu^t_{\varepsilon+\hbar\omega_0-\varepsilon_B,\varepsilon} f_{\varepsilon+\hbar\omega_0-\varepsilon_B} - \nu^t_{\varepsilon-\hbar\omega_0+\varepsilon_B,\varepsilon} f_\varepsilon = 0, \quad \varepsilon_B - \hbar\omega_0 < \varepsilon < \hbar\omega_0, \tag{A5}$$

and χ_ε is determined by the system

$$\frac{df_\varepsilon}{d\varepsilon} = -(\nu_m + \nu_{\varepsilon-\hbar\omega_0+\varepsilon_B,\varepsilon})\chi_\varepsilon, \quad 0 < \varepsilon < \varepsilon_B - \hbar\omega_0,$$

$$\frac{df_\varepsilon}{d\varepsilon} = -(\nu_m + \nu_{\varepsilon-\hbar\omega_0+\varepsilon_B,\varepsilon})\chi_\varepsilon + \tilde{\nu}_{\varepsilon+\hbar\omega_0-\varepsilon_B,\varepsilon}\chi_{\varepsilon+\hbar\omega_0-\varepsilon_B}, \quad \varepsilon_B - \hbar\omega_0 < \varepsilon < \hbar\omega_0. \tag{A6}$$

*ajhernan@ull.es
†ftvasko@yahoo.com

[1] R. F. Kazarinov and R. A. Suris, Sov. Phys. Semicond. **5**, 707 (1971) [Fiz. Tekh. Poluprovodn. (S.-Peterburg) **5**, 797 (1971)]; R. A. Suris and B. S. Shchamkhalova, Sov. Phys. Semicond. **18**, 738 (1984) [Fiz. Tekh. Poluprovodn. (S.-Peterburg) **18**, 1178 (1984)].

[2] L. L. Bonilla and H. T. Grahn, Rep. Prog. Phys. **68**, 577 (2005); R. C. Iotti and F. Rossi, *ibid.* **68**, 2533 (2005); A. Wacker, Phys. Rep. **357**, 1 (2002).

[3] R. Kohler, A. Tredicucci, F. Beltram, H. E. Beere, E. H. Linfield, A. G. Davies, D. A. Ritche, R. C. Iotti, and F. Rossi, Nature (London) **417**, 156 (2002); A. Tredicucci, R. Kohler, L. Mahler, H. E. Beere, E. H. Linfield, and D. A. Ritchie, Semicond. Sci. Technol. **20**, S222 (2005).

[4] J. Faist, D. Hofstetter, M. Beck, T. Aellen, M. Rochat, and S. Blaser, IEEE J. Quantum Electron. **38**, 533 (2002); C. Gmachl, F. Capasso, D. L. Sivco, and A. Y. Cho, Rep. Prog. Phys. **64**, 1533 (2001).

[5] M. S. Vitiello, V. Spagnolo, G. Scamarcio, A. Lops, Q. Yang, C. Manz, and J. Wagner, Appl. Phys. Lett. **90**, 121109 (2007); M. S. Vitiello, G. Scamarcio, V. Spagnolo, C. Worral, H. E. Beere, D. A. Ritchie, C. Sirtori, J. Alton, and S. Barbieri, *ibid.* **89**, 131114 (2006).

[6] C. Jirauschek, G. Scarpa, P. Lugli, M. S. Vitiello, and G. Scamarcio, J. Appl. Phys. **101**, 086109 (2007).

[7] M. S. Vitiello, G. Scamarcio, J. Faist, G. Scalari, C. Walther, H. E. Beere, and D. A. Ritchie, Appl. Phys. Lett. **94**, 021115 (2009).

[8] F. T. Vasko and A. V. Kuznetsov, *Electron States and Optical Transitions in Semiconductor Heterostructures* (Springer, New York, 1998).

[9] V. F. Elesin and E. A. Manykin, JETP Lett. **3**, 15 (1966); Sov. Phys. JETP **23**, 917 (1966); V. F. Elesin, Phys. Usp. **48**, 183 (2005); H. J. Stocker, Phys. Rev. Lett. **18**, 1197 (1967).

[10] A. C. Durst and S. H. Girvin, Science **304**, 1752 (2004); V. I. Ryzhii, Phys. Usp. **48**, 191 (2005); S. I. Dorozhkin, *ibid.* **48**, 198 (2005).

[11] F. T. Vasko, JETP Lett. **79**, 431 (2004); O. E. Raichev and F. T. Vasko, Phys. Rev. B **73**, 075204 (2006).

[12] R. G. Mani, J. H. Smet, K. von Klitzing, V. Narayanamurti, W. B. Johnson, and V. Umansky, Nature (London) **420**, 646 (2002); M. A. Zudov, R. R. Du, L. N. Pfeiffer, and K. W. West, Phys. Rev. Lett. **90**, 046807 (2003).

[13] F. T. Vasko and O. E. Raichev, *Quantum Kinetic Theory and Applications* (Springer, New York, 2005).

[14] E. M. Lifshitz and L. P. Pitaevskii, *Physical Kinetics* (Pergamon, Oxford, 1981).

[15] In Fig. 3 for $T_{\rm ph}=4.2$ K the initial distribution function $f_{1\varepsilon=0}\simeq 0.11$ (if $T=5$ meV and $\nu_m=1$ ps^{-1}), 0.09 (if $T=5$ meV and $\nu_m=0.5$ ps^{-1} or if $T=3.5$ meV and $\nu_m=1$ ps^{-1}), and 0.07 (if $T=3.5$ meV and $\nu_m=0.5$ ps^{-1}). For $T_{\rm ph}=20$ K, $f_{1\varepsilon=0}\simeq 0.045$ (if $T=5$ meV and $\nu_m=1$ ps^{-1}), 0.033 (if $T=5$ meV and $\nu_m=0.5$ ps^{-1} or if $T=3.5$ meV and $\nu_m=1$ ps^{-1}), and 0.025 (if $T=3.5$ meV and $\nu_m=0.5$ ps^{-1}).

[16] P. Hyldgaard and J. W. Wilkins, Phys. Rev. B **53**, 6889 (1996); M. Hartig, J. D. Ganiere, P. E. Selbmann, B. Deveaud, and L. Rota, *ibid.* **60**, 1500 (1999); K. Kempa, P. Bakshi, J. Engelbrecht, and Y. Zhou, *ibid.* **61**, 11083 (2000).

[17] P. Kinsler, R. M. Kelsall, and P. Harrison, Physica B **263-264**, 507 (1999).

[18] H. Haken, *Synergetics* (Springer, Berlin, 1983); E. Scholl, *Nonequilibrium Phase Transitions in Semiconductors* (Springer, Berlin, 1987).